



Multi-devices field magnetic susceptibility: '3D' spatialization of metallic contamination in soils and reverse correlation in carbonated context (Jebel Ressas, Tunisia)

Sonia Rousse¹ · Muriel Llubes¹ · Manel Ghorbel² · Marilyne Soubrand³ · Emmanuel Joussein³ · Marguerite Munoz¹

Received: 5 September 2022 / Accepted: 11 August 2023 / Published online: 8 September 2023
© The Author(s) 2023

Abstract

Soil contamination linked to abandoned lead–zinc mining wastes represents a serious environmental hazard of worldwide concern, raising the need for cost-effective tools to spatialize the contaminated area and assess the risks. In worldwide industrial environments, positive correlation between magnetic susceptibility and heavy metal soil contamination is often reported and used for fast preliminary site assessments. In this study, we report monitoring of an olive grove, situated below one of the abandoned tailings dump of the former Jebel Ressas Pb–Zn mining site (Tunisia), with three different commercial susceptibilimeters (Terraplus KT10, Bartington MS2D and Geonics EM38 induction device). Integration depths of above-mentioned susceptibilimeters vary from 3 to 150 cm. Similar broad-scale magnetic susceptibility maps for the three devices emphasize the effect of topography and runoff transfer as the main mechanisms for tailings material dispersion. Very low susceptibilities ($\sim 10 \times 10^{-5}$ SI) characterize the contaminants magnetic signal, while uncontaminated soils susceptibilities are one order of magnitude higher ($100\text{--}150 \times 10^{-5}$ SI). This unique case of reverse correlation between magnetic susceptibilities and contamination (Pb, Zn, Cd) trace efficiently the degree of contamination and is substantiated by further mineralogical and magnetic properties analyses showing the predominance of iron amorphous oxyhydroxides in the dump, while (titano) maghemite is the main natural magnetic carriers in the uncontaminated soils in this specific carbonated context. The Geonics EM 38, with a proper calibration procedure, reveals a performant tool increasing the depth of investigation and when combined with shallower susceptibilimeter, opens perspectives for qualitative 3D spatialization of metallic contamination.

Keywords Magnetic susceptibility · Metallic contamination · 3D spatialization · Geonics EM38 · Reverse correlation · Carbonated context

Introduction

Among the modern societal concerns, the environmental quality and its impact on human health have become major challenges. It has been demonstrated that heavy metals have

non-negligible impacts on ecosystems, and hence on living and health conditions (see, for example, Berntsen et al. 2010; Hansard et al. 2011). Metals can migrate from the source of contamination to soil via several physical–chemical transfer mechanisms (Kabata-Pendias and Pendias 1992). If the source is not isolated, contaminants may reach the biosphere (Kabata-Pendias 2004) and accumulate up to and above thresholds of toxicity for human's health (see, for example, Gutiérrez et al. 2016; Ding et al. 2018; Monneron-Gyurits et al. 2020). Cadmium (Cd) and lead (Pb) are common pollutants which have, to different degree, a relationship with many pathological states such as renal and bones damage, growth and neurobehavioral problems, high blood pressure and even, potentially, cancer (Kabata-Pendias and Pendias 1992; USEPA 2012). Zinc (Zn), although being an essential oligoelement, also becomes toxic at very high doses especially on immunity and digestive systems (Fosmire 1990).

✉ Sonia Rousse
sonia.rousse@get.omp.eu

¹ Géosciences Environnement Toulouse (UMR5563, IRD, Université Toulouse III), 14 Avenue Edouard Belin, 31400 Toulouse, France

² Laboratoire de Traitement et de Valorisation des rejets hydriques (LTVRH), Centre de Recherche et de Technologie des Eaux (CERTe) Technopole Borj-Cedria, BP No 273, 8020 Soliman, Tunisia

³ Université de Limoges, E2Lim UR24133, 123 Avenue Albert Thomas, 87060 Limoges Cedex, France

These heavy metals must be considered as potentially hazardous substances (PTEs) inducing a risk to human health (Adriano 2001).

Countries from the Mediterranean southern riverside display large mine tailings quantities rich in heavy metals like Pb, Cd, Zn, Sb, As and Hg coming from mining sites abandoned or still in activity (Gutiérrez et al. 2016). For the majority of these sites, villages and farmlands developed adjacent to the treatment plant. Health risk assessment linked with waste metallic particles depends upon multiple and complex interactions of several parameters such as waste mineralogy, climatic conditions and contamination transfer, time elapsed since mine closure, land use, local population practices and type of remediation, if undertaken, to reduce impacts of contamination (Johnson et al. 2000; Passariello et al. 2002; Dumas et al. 2018; Gutiérrez et al. 2016). In Tunisia, around 50 mining sites have been exploited leaving important volumes of mine tailings for which high concentrations in Pb, Cd, and Zn have been evidenced (Ghorbel et al. 2010; Othmani et al. 2013; Boussen et al. 2013; Daldoul et al. 2015; Souissi et al. 2015; Pascaud et al. 2015; Sliiti et al. 2019). Despite the absence of acid drainage linked to the carbonated context, the fine granulometry, the light cohesion, the absence of vegetation cover and the lack of specific remediation actions render these tailings particularly vulnerable to hydric and aeolian erosion processes notably linked to intense and time-limited climatic events (high-speed winds and heavy rainfall) characteristic of the semi-arid climate of this region. Therefore, miner's villages built adjacent to former treatment plants and surrounding farmlands have often undergone historical accumulation of metals in soils, generating exposure of inhabitants via different pathways (Ghorbel et al. 2010, 2014; Ghorbel 2012; Daldoul et al. 2015; Béjaoui et al. 2016; Pascaud et al. 2015).

Recognition of contaminated areas generally rely on time-consuming procedures based on numerous sampling followed by expensive geochemical analyses. Development of indirect methods such as geophysical measurements emerged in the last decade as a valuable tool for contamination spatialisation and first assessments of principal mechanisms responsible for tailings dispersion (Steeles 2001; Pérez et al. 2014; Pierwola et al. 2020). Magnetic methods combined with magnetic mineralogy and selected geochemical analyses have proven their efficiency in tracking heavy metal contamination both in urban and industrialized zones worldwide (see, for example, Schmidt et al. 2005; Maher 2009; Jordanova et al. 2010, 2013; Wang 2013). This technique presents the advantage of being quick, easy to operate, and cost-effective. Almost generally, positive correlations between magnetic susceptibilities and heavy metal (Pb, Cd, Zn, As, etc.) concentrations are found, explained by the ability of Fe-oxides, often associated with the waste generated by the metallurgical processes or derived from the ore after

weathering, to retain potential toxic elements on their surface due to sorption processes (i.e., Pérez et al. 2014 and references therein). However, for each given context, the relationship between the soil's heavy metal contamination and the magnetic mineralogy needs to be assessed.

In this experiment designed before the release of the ISO 21226:2019, we present a rare case of reverse correlation between metallic contamination and magnetic susceptibility from a former Pb–Zn mining site in North-Eastern Tunisia (see Fig. 1A). We focused our detailed contamination study on an olive grove situated next to a flattop waste dump nearby the former miner's village of Jebel Ressas (Dump III, Fig. 1; Ghorbel et al. 2010; Souissi et al. 2015). To spatialize the contamination, we tested the reliability of three commercial susceptibilimeters (GEONICS EM38, Bartington MS2D sensor; Terraplus KT10) the two latter being commonly used to measure magnetic susceptibility in environmental studies. The three devices mainly differ in their integration depths varying from 150 cm for the deepest GEONICS EM38 to 3 cm for the shallowest Terraplus KT10. To better assess the origin of our susceptibility signal, we completed our in situ study with laboratory magnetic mineralogy and portable X-ray fluorescence analyses of soils and mining wastes sampled in the field.

Materials and methods

Site description and sampling

The village of Jebel Ressas, located about 30 km southeast of Tunis (36° 36' 33.02", 10° 18' 56.58", Fig. 1A), developed close to an ancient extraction Pb–Zn site, at the foot of the Jebel Ressas mountain (literally the lead mountain). Pb and Zn ores are hosted in the Jurassic calcareous layers and are composed of Pb, Zn, and Fe sulfides (galena, sphalerite and pyrite) with abundant secondary minerals, Pb–Zn bearing carbonates, silicates and iron oxides hosted in the limestones (Sainfeld 1952; Jemmali et al. 2011). The village involves an area of 0.07 km² with a few hundreds of inhabitants and expands southwards by and westwards on the contaminated area of the ore-processing plant where the ore was ground and concentrated. Extraction and subsequent ore treatment between 1880 and 1956 resulted in almost two millions of tons of gravimetry and flotation wastes dumped in three distinct flat top heaps (see Fig. 1b in Ghorbel et al. (2010) for respective location of DI, DII, and DIII). The northernmost heap DIII (Fig. 1B) is the largest one (about 35, 250 m²) with mean concentrations of the waste material of 7.11 wt% for Zn, 2.3 wt% for Pb and 290 mg/kg for Cd (Ghorbel et al. 2010). No vegetation has grown on the dump. The waste material exhibits a weak cohesion and fine grain size dominated by silts and clay and no specific remediation action

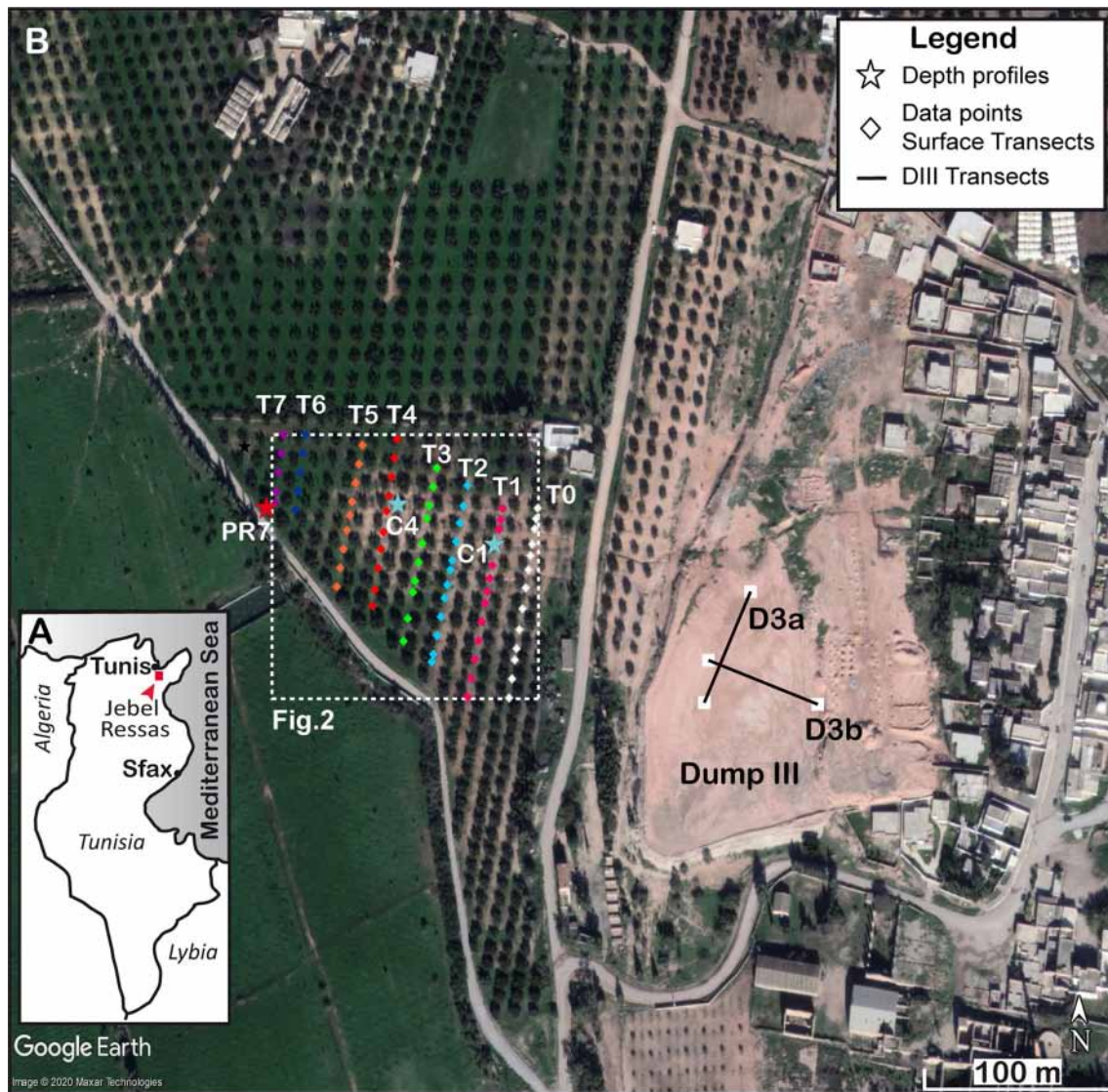


Fig. 1 Setup of the study. **A** Location map of Jebel Ressay Village. **B** Google Earth image with location of the geophysical study (White dotted square). Part of Jebel Ressay village is observable on the East of Dump III. Blue stars correspond to the depth profiles from this

was undertaken to prevent erosion and/or chemical alteration (Ghorbel et al. 2010).

Westerly and north-westerly winds prevailed in the region and favor contaminated dust transfer from Dump III towards the village (Fig. 1B). However, simulations of metal contamination in aerosols during the summer period by Ghorbel et al. (2014) have shown spreading of contamination towards agricultural lands to the North West of the dump (and notably toward the olive grove investigated in this study) by easterly stronger winds more efficient for dust emission and transfer. The annual precipitations average slightly less than 500 mm but under the Mediterranean climate occur generally as heavy storms, which favor the

study, Red star materialize the localization of the soil profile of Souissi et al. (2015) (see text). Colored Diamonds show individual data points

runoff transport (Dumas et al. 2018). This contamination transfer mechanism impacted the olive grove investigated in this study, situated downslope West of dump DIII (Fig. 1B) and characterized by a topographic depression in its center, with field evidences of runoff from the dump toward this depression (Ghorbel 2012).

Our in situ magnetic susceptibility measurements were performed along eight parallel transects separated by 20 m on average in the olive grove to the North West of dump DIII (Fig. 1). Along the transects T0 (100 m), T1 (100 m), T2 (100 m), T3 (90 m), T4 (90 m), T5 (75 m), T6 (45 m), and T7 (40 m), measurements were taken every 10 m on average. Locally, additional measurements (5 on average /transect)

Fig. 2 Volumic susceptibility maps of the Olive grove along the profiles of Fig. 1. **a** With the Terraplus KT10; **b** with the Bartington MS2D, and **c** with the Geonics EM38. Localization units are UTM. The color scale is the same for the three maps

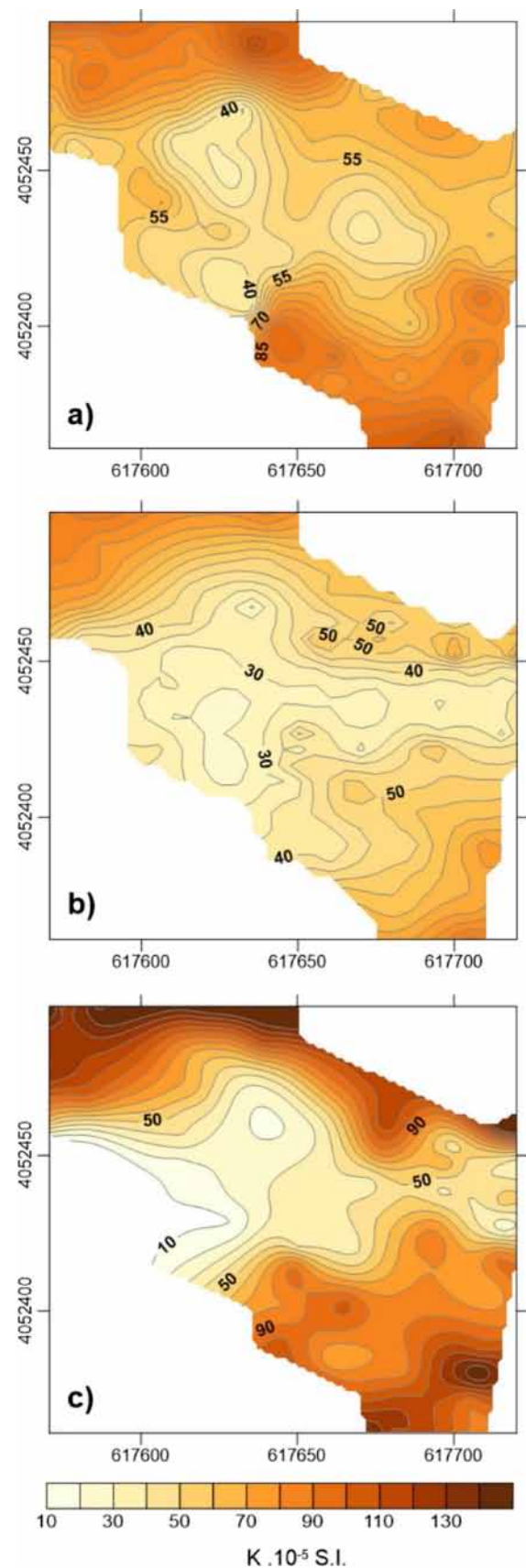
were realized to assess the reliability of the observed variations and avoid disturbances linked to small metallic particle waste unrelated with our investigation goals. Two perpendicular transects (Fig. 1B) were also measured on dump DIII topmost surface (only with Bartington MS2D sensor device) to assess the level and variability of the susceptibility measurements linked to the most contaminated surfaces. In the field, for all points taken with the Bartington MS2D probe, three distinct measurements were averaged to account for the variability linked with soil surface irregularities and prevent potential unrepresentative metallic contamination. All the profiles were positioned with GPS then transferred to UTM coordinates (Fig. 2).

In addition to the field measurements, samples of the soil surface (1–2 kg on average) were taken at each point along four transects (T1, T4, T6, T7) in the olive grove. Samples were stored in plastic bags and then re-conditioned in the laboratory in plastic pills and cubes to allow the magnetic properties measurements after drying in the air for a few days. Two depth profiles (C1 (maximum depth 30 cm), C4 (maximum depth 52 cm; Fig. 1.) were also sampled with an auger to test the soil impregnation depth to contamination. For profile C1, only two soil samples could be retrieved at 4 and 23 cm depth (± 1.5 cm); whereas for C4, samples were taken at 5, 20, 29, 38, and 48 cm depth (± 1.5 cm).

Mineralogy of Dump III and adjacent soils

Ghorbel et al. (2010) have shown that calcite is the most representative mineral in the Jebel Ressas mining waste. Presence of ankerite ($\text{Ca}(\text{Mg}, \text{Fe})(\text{CO}_3)_2$) is also detected. The clay minerals are principally kaolinite ($\text{Al}_2\text{Si}_2\text{O}_5(\text{OH})_4$) and illite ($\text{KA}_2\text{Si}_3\text{AlO}_{10}(\text{OH})_2$). The metallic bearing phases (Pb, Zn, and Cd) are in majority carbonates (cerusite (PbCO_3), smithsonite (ZnCO_3), and hydrozincite ($\text{Zn}_5(\text{OH})_6(\text{CO}_3)_2$)), silicates (hemimorphite ($\text{Zn}_4\text{Si}_2\text{O}_7(\text{OH})_2(\text{H}_2\text{O})$), and willemite (Zn_2SiO_4)), sulfides (galena, sphalerite, pyrite) and iron oxyhydroxides. Cadmium appears as zinc substitution in the different species of zinc minerals. The chemical composition and the absence of signal in the XRD converge to the idea that the iron oxyhydroxides are mainly amorphous, such as ferrihydrite, and high pH (characteristic of alkaline carbonated environments) like lepidocrocite or goethite (Pankhurst and Pollard 1992; Liu et al. 2007). No hematite was identified in the mineralogical analyses of Dump III.

According to Souissi et al. (2015), clay and silt principally compose the soils near Dump III where kaolinite, illite, calcite dolomite, and quartz dominate. For the soils along



radial referred as R8, which cross our field investigation area to the West of Dump III, hemimorphite, cerussite, barite, and hydrozincite are also present. Along this radial, Souissi et al. (2015) report the highest contents of Zn, Pb, and Cd (6.65%, 2.39%, and 296 mg/kg respectively). Iron oxyhydroxides represent around 3% (samples PR6 and PR7) of the mineral phases in the soils without further characterization (Souissi et al. 2015). Values of 57, 3814, and 9203 mg/kg for Cd, Pb, and Zn, respectively, are also reported in our area of investigation (Sample P3, Elouear et al. 2016).

Magnetic susceptibility datasets

Volumic magnetic susceptibilities (κ) were measured in situ with two field susceptibilimeters (Bartington MS2D sensor, and Terraplus KT10).

We also performed susceptibility measurements (κ) with a GEONICS EM38 electromagnetic induction (EMI) device. This instrument is usually devoted to conductivity surveys but can also be used to map qualitative variations of field susceptibility (De Smedt et al. 2014). To obtain quantitative measurements, an additional calibration is necessary. We used the protocol described in Thiesson et al. (2016) using theoretical calculation from a ground layer with different susceptibilities. First, we took a non-magnetic purely conductive aluminum sphere to find the converting coefficient between field measures and ppm (part per million). For our instrument, the adjusted coefficient is 35 ppm (from the secondary field over the primary field ratio), to be compared to the coefficient of 29 ppm indicated in the user's manual of GEONICS. Second, we calibrated the electromagnetic response of the device to convert ppm values into real susceptibility values. Using our calibration results, we re-calculated the data obtained in the field. The goal was to test the reliability of this device and method in comparison with more classical near surface susceptibilimeters. With this protocol, this instrument integrate volumetric susceptibility measurements at greater depth than the other devices.

Measurements with the GEONICS EM38 and Bartington MS2D were realized simultaneously in May 2012. The Terraplus KT10 measurements were realized the same year during a second field campaign using the same profiles and position. The three instruments differ mostly by the volume on which the susceptibility (measured in SI) is integrated. The effective penetration depth is considered to be 6–8 cm for the MS2D sensor (diameter of 164 mm) corresponding to 90% of the recorded signal (Lecoanet et al. 1999) and about 3 cm for the KT10 (diameter of 65 mm). The sensitivity is similar for the KT10 and the MS2D on the order of 1.10^{-6} SI. Variations in surface susceptibility values measured with the Bartington MS2D and Terraplus devices are ascribed to their different penetration depths revealing magnetic properties inhomogeneity in the media investigated (Jordanova

et al. 2003). In comparison, for the GEONICS EM38, the depth of response is supposed to be up to 150 cm with a sensitivity on the order of 10^{-5} SI.

To investigate the instrumental responses produced by the different devices, we realized the measurements following the principle of a square pattern in an olive grove situated below and to the West of dump III (see Fig. 2). It is worth to note here that the olive grove is plowed almost every 6 months up to a depth estimated by the farmer at 40–60 cm. The measurements with the MS2D susceptibilimeter, EM38 device and the sampling was realized before plowing of the field whereas, those with the KT10 susceptibilimeter were done shortly after. Maps for each of the concerned devices were drawn with the commercial SURFER Software (<https://www.goldensoftware.com/products/surfer>) using minimum curvature interpolation. Unfortunately, a technical failure prevented the in situ measurements of the T6 and T7 profiles with the Bartington MS2D sensor. However, soil samples were taken at each measurement point of these two profiles as well as for profiles T4 and T1 to perform the laboratory magnetic analyses (see Sect. 3). In the light of the results obtained on the soil samples (see “Magnetic properties and anti-correlation with contamination”), we built a composite map (combining in situ and laboratory measurements) to allow a better visualization and comparison of the results, even if, therefore, the westernmost part of the map has to be taken with more caution (see Sect. 3 for explanation and discussion).

Magnetic properties and portable X-ray fluorescence (pXRF) analyses

Magnetic properties investigations were performed at the GET (Toulouse, France), IPGP (Paris, France), and LFC (Pau, France) Magnetism Laboratories.

On the sampled soils, after resampling in cubes of 11 cm^3 , low field volumic susceptibility κ was measured first with a Kappabridge KLY3 (AGICO) susceptibilimeter to compare with results obtained directly in the field. Then, low (0.465 kHz) and high (4.65 kHz) frequencies of the mass-normalized magnetic susceptibility were measured with a Bartington MS2B frequency sensor. Frequency-dependent susceptibility ($\chi_{fd\%} = 100 \times (\chi_{if} \chi_{hf}) / \chi_{hf}$) is a widely used normalized parameter reflecting magnetic particles with grain sizes close to the superparamagnetic/single domain (SP/SD) boundary (Verosub and Roberts 1995). The high percentage levels of (SP/SD) found with the Bartington MS2B sensor (see “Magnetic properties and anti-correlation with contamination”) lead us to realize complementary measurements with a more sensible AGICO MFK1 Kappabridge following the procedure defined in Hroudá et al. (2013, 2015) to obtain the numerically equivalent χ_{on} normalized parameter

($\chi_{\text{on}} = (200/\pi) \tan\delta$, where δ is the phase angle (Jackson 2003).

To assess the different components of the magnetic mineralogy, we performed temperature-dependent magnetic susceptibilities K–T curves, under Argon atmosphere, using a CS3 high-temperature unit attached to a KLY3 Kappabridge (AGICO).

To explore the conjugate variations between contamination and magnetic signal, measurements of elemental occurrences for Pb, Zn, and Cd were realized in the GET (Toulouse, France) using a portable Bruker's XRF S1 Titan spectrometer on the same soils samples used for magnetic properties in the laboratory (Profiles T1, T4, and depth profile C4). Measurements protocol follow the ex situ protocol described in Horta et al. (2015). The external reproducibility of the method is addressed by repeated measurements of international standard NIST 44 (National Institute for Standards and Technology) throughout the analytical session (every 5 measurements on average) with certified values of 330 ± 48 mg/kg and 656 ± 75 mg/kg for Pb and Zn, respectively. Over 8 measurement a calculated mean of 308.5 mg/kg (mean error of 6.5% and mean reproducibility of 96%) and 639.5 mg/kg (mean error of 2.5% and mean reproducibility of 91%) was found for Pb and Zn, respectively, with a calculated 2σ deviation of 8% for Pb and 18% for Zn.

Results and interpretations

Spatial distribution of magnetic susceptibilities

After characterizing the background susceptibility signal on the uncontaminated soil matrix about 3 km away from Dump III, which gave value of $100\text{--}150 \times 10^{-5}$ SI, susceptibilities were first measured on DIII dump top along a 60 m long transect to define the contaminated surface susceptibility response (Fig. 1B). Susceptibilities measured each 10 m with the Bartington MS2D probe on D3a (Fig. 1B) range between 9 and 13.3×10^{-5} SI with an average of 10.7×10^{-5} SI. These low values suggest the quasi absence of ferromagnetic phases in the mineralogical assemblage of the dump. Similar values ($9.3\text{--}12.25 \times 10^{-5}$ SI with an average of 10.6×10^{-5} SI) are observed for the 60 m long perpendicular transect (D3b—Fig. 1B) even if even shallower levels of susceptibility ($2\text{--}5 \times 10^{-5}$ SI) associated with a visible unanalyzed dark crust are also encountered. These measurements are consistent with the presence of lepidocrocite or goethite for which typical susceptibilities are on the order of a few 10^{-5} SI and amorphous iron oxyhydroxides as already suggested by the mineralogical studies (Ghorbel et al. 2010).

Figure 2 shows the spatial distribution of the susceptibilities in the olive grove obtained with the three different devices used. The three datasets are plotted using the

SURFER10 software using minimum curvature interpolation and the same color scale for direct comparison. Measured susceptibilities range between 17 and 108×10^{-5} SI, 31 and 114×10^{-5} SI, and 10 and 159×10^{-5} SI for the Bartington MS2D, KT10, and EM38, respectively. Similar ranges are observed for the variations with the MS2D and KT10 and slightly higher for the EM38 interpreted as due to the penetration differences and soil volumes integrated by the different devices.

Recalling that the unpolluted susceptibility background signal is around $100\text{--}150 \times 10^{-5}$ SI, the one order of magnitude lower susceptibilities obtained directly on the mine tailing show that soil contamination is most probably evidenced in this study by a decrease in magnetic susceptibilities. Magnetic susceptibility and level of contamination are, therefore, here anti-correlated contrary to what is usually expected for metallic contamination (i.e., Evans and Heller 2003; Chaparro et al. 2007; Dankoub et al. 2012; Wang 2013). Further evidences of this strong anti-correlation are described in “[Magnetic properties and anti-correlation with contamination](#)”, and Fig. 3.

The first-order coherency of the patterns displayed is similar despite some variations in sensibility and/or penetration of the different tools. KT10 and to a lesser extent Bartington susceptibilimeters probably due to their shallow penetration depth seem more influenced by high-frequency disturbances linked to soil asperities, shallow and localized variations of lithology and/or small and shallow metals particles. Plowing of the field seems to have a limited effect on the repartition of the anomalies. All maps show a non-uniform distribution of the magnetic susceptibilities. Contaminants seems to accumulate in a central zone on the olive grove corresponding to a topographic depression zone in the field and along two pathways linking this depression zone to the dump slope and corresponding to streaming water line (or temporary brooks) also identified in the field. Despite the undeniable contribution by eolian transfer (Ghorbel et al. 2014), the main mechanism for contamination transfer toward these agricultural zones is most probably, therefore, linked to runoff transfer.

Anomalous low susceptibilities can be detected with the geophysical measurements more than 200 m away from the dump. Using the progressive penetration depths of the devices used, we observed that the contamination maximize below 3 cm and tend to fade away at 150 cm, apart in the central depression where it accumulates. It is worth to note that the influence of soil moisture is negligible on magnetic susceptibility measurements contrary to other geophysical investigations methods (Maier et al. 2006; Pierwola et al. 2020) and, therefore, that the signal cannot be biased by the water content.

Comparison of the results maps obtained with the three devices allows us to validate the use of the Geonics EM38

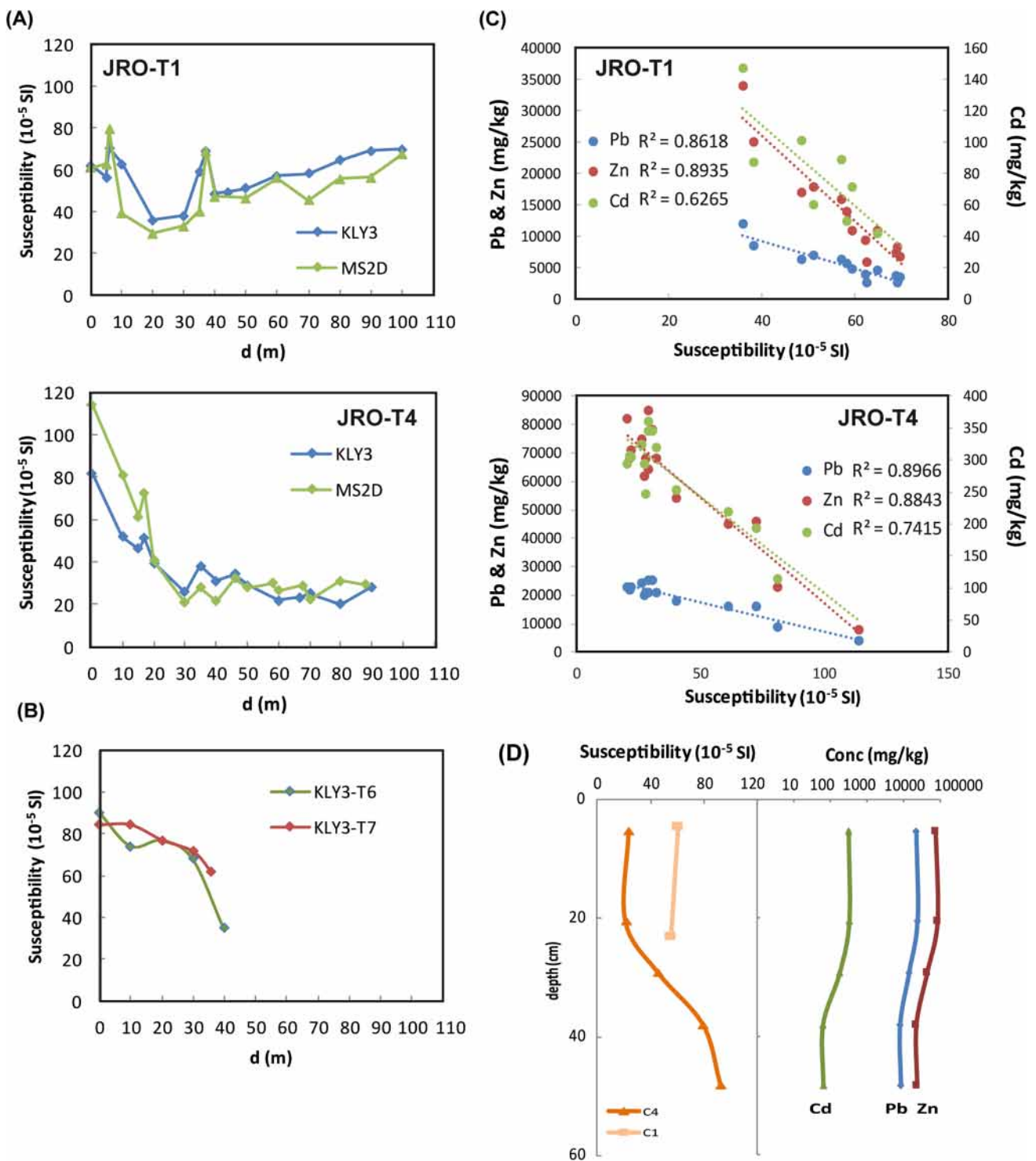


Fig. 3 **A** ‘In situ’ (Bartington MS2D) and laboratory (hand-samples AGICO-KLY3) volumic susceptibility measurements along profiles T1 and T4. **B** Hand sample’s volumic susceptibilities for profiles T6 and T7 incorporated in the ‘composite’ Bartington MS2D map of Fig. 2 after failure of this latter device in the field. **C** pXRF elemental concentration in mg/kg for Pb, Zn, and Cd versus AGICO-KLY3

volumic magnetic susceptibilities for profiles T1 and T4 exhibiting strong anti-correlation. Associated determination coefficients are displayed. **D** AGICO-KLY3 volumic susceptibilities versus depth on profiles C1 and C4 measured in the laboratory and conjugate pXRF elemental concentration for Pb, Zn, and Cd versus depth on profile C4

as a quantitative field susceptibilimeter, granted that calibration is properly done following the procedure described in Thiesson et al. (2016). The combination of the devices with different penetration depths also opens the possibility for qualitative 3D mapping of contaminated area.

Magnetic properties and anti-correlation with contamination

To interpret the susceptibilimeters record and characterize the magnetic carriers involved, magnetic properties investigations and pXRF measurements were conducted at the GET magnetism Laboratory (Table 1). Susceptibilities (χ) of surface samples from 4 profiles (T1, T4, T6, and T7) and two depth profiles were measured with a KLY3 (AGICO) susceptibilimeter. Along profiles T1 and T4, results display a very good agreement between the Bartington field MS2D sensor measurements and the sub-surface samples taken at the same points (Fig. 3). Determination coefficients (R^2) of 0.7 and 0.8 are, respectively, found (Fig. 3). This result allowed us to use the laboratory susceptibilities measured for T6 and T7 (Fig. 3B) to build the 'Bartington' composite map of Fig. 2 and palliate to the technical failure of the Bartington susceptibilimeter in the field. The coherency between the laboratory and field measurements is also encouraging to consider the latter as representative of the magnetic mineralogy present in the field.

To evidence the relation between contamination and magnetic susceptibilities, pXRF values for Pb, Zn, and Cd realized on soils sampled on profiles T1 and T4 were plotted against the AGICO-KLY3 susceptibilities realized on the same sampled soils (Fig. 3C). Determination coefficients (R^2) of 0.86 (T1) and 0.9 (T4) are found for the anti-correlation with Pb, 0.9 (T1) and 0.88 (T4) for Zn, and a slightly lower anti-correlation is found for Cd with R^2 values of 0.63 (T1) and 0.74 (T4) (Fig. 3C). Even if pXRF might be sensible to soil moisture and heterogeneities of the soil matrix, Horta et al. (2015) showed doing pairwise comparison pXRF and ICP-AES that pXRF was highly applicable to measure Pb and Zn while potentially less accurate for Cd. It is worth to note that Pb, Zn, and Cd concentrations found with pXRF in this study are very similar to concentrations reported for the same olive groove (Souissi et al. 2015; Elouear et al. 2016).

The most detailed depth profile C4 show that susceptibilities start to increase below 20 cm depth to reach values close to $80\text{--}100 \times 10^{-5}$ SI at 40–50 cm on the order of the unpolluted matrix susceptibilities (Fig. 3D). The pXRF values again substantiate the strong anti-correlation between susceptibility and contamination even at depth with R^2 above 0.9 for the three elements considered (Pb, Zn and Cd) and a clear decrease of contamination in Pb, Zn, and Cd at depth. These results reinforce the interpretation of the geophysical

measurements based on the penetration depths of the different devices. The combined data show that the highest soil contamination degree by the mine tailing is restrained to the 20–25 cm first centimeters and then tend to diminish to become almost undetectable with magnetic susceptibilities below 50 cm depth, which is approximately the depth of the plowing estimated by the farmer.

Figure 4 shows examples of representative temperature-dependent magnetic susceptibilities (K–T curves) from top of dump III (A) representative of the mine tailing and the olive grove (B) surface samples. Realized in argon atmosphere, all curves exhibit an irreversible behavior probably linked to a change in mineral phases during heating (Tauxe 1998, 2005). For DIII K–T curve (Fig. 4A), the absence of susceptibility signal up to 350 °C is coherent with the predominance of amorphous iron oxyhydroxides and/or lepidocrocite inferred from the mineralogical studies ("Mineralogy of Dump III and adjacent soils"). The curve display a Curie temperature (T_c) of 592 °C as determined by the tangent method (Petrovsky and Kapicka 2006). Transformation of lepidocrocite into maghemite upon heating as described by Gendler et al. (2005) would explain the change in slope in the heating susceptibility curve observed around 510 °C (Fig. 4A) and the later presence of hematite absent from the mineralogical studies. Although maghemite ($\gamma\text{-Fe}_2\text{O}_3$) has the same composition as hematite ($\alpha\text{-Fe}_2\text{O}_3$), it has the structure of a spinel (a cation-deficient spinel, lacking sufficient Fe^{3+} ions to fill the available Fe sites) and is ferrimagnetic. It is metastable with respect to hematite and therefore inverts to hematite upon heating which is coherent with the progressive decrease delineated by a low slope between 600 and 680 °C, suggesting the presence of maghemite and/or hematite (Tauxe 1998; Evans and Heller 2003).

For the Olive grove sample taken on the T4 profile (Fig. 4B), similar features, though less pronounced, are observed, attesting the contamination by the mine tailing. However, the presence of a susceptibility signal at low temperatures and the progressive decrease of this signal between 250 and 440 °C plus the lowering of the main T_c to 572 °C, indicate the presence of additional magnetic carriers, probably titanomaghemite (or partially oxidized titanomagnetite), initially originating from the unpolluted soil. Titanomaghemite is unstable over heating and inverts to rhombohedral hematite ($\alpha\text{-Fe}_2\text{O}_3$) at temperatures between 250 and 750 °C (Özdemir 1990). These titanomaghemites probably originate from slow oxidation under ambient conditions of titanomagnetites, a process also often called maghemitization frequently reported in soil (Dunlop and Özdemir 2001; Soubrand-Colin et al. 2009).

The frequency-dependent magnetic susceptibility $\chi_{fd\%}$ is used to indicate the occurrence and abundance of ultrafine superparamagnetic (SP) magnetic particles (Dearing et al. 1996; Evans and Heller 2003). Measurements of the $\chi_{fd\%}$

Table 1 Volumic magnetic susceptibilities κ measured with AGICO-KLY3 and pXRF concentrations for Pb, Zn, and Cd obtained with Bruker's XRF S1 Titan spectrometer on depth profiles C1 and C4 and surface profiles T1 and T4

Samples	K (10^{-5} SI)	Depth (cm)	Pb (mg/kg)	Zn (mg/kg)	Cd (mg/kg)
Depth profiles					
C1–20	60.37	4.61	3770	9173	bdl
C1–100	55.51	23.08	3006	6908	bdl
C4–18	24.07	5.26	22000	73000	320
C4–70	21.56	20.45	24000	82000	335
C4–100	45.87	29.21	14000	43000	184
C4–130	79.02	37.98	7928	22000	64
C4–165	92.08	48.2	8337	23000	65
Surface profiles					
T1					
T1–0	62.16		3875	9336	bdl
T1–10	62.67		2646	6002	bdl
T1–20	36		12000	34000	147
T1–30	38.23		8651	25000	87
T1–35	59.42		4755	11000	72
T1–37	69.15		2753	8399	bdl
T1–40	48.65		6456	17000	101
T1–50	51.24		6993	18000	60
T1–60	57.02		6417	16000	89
T1–70	58.24		5727	14000	50
T1–80	64.73		4661	11000	42
T1–90	68.99		3771	7540	bdl
T1–100	69.7		3610	6849	bdl
T4					
T4–0	114.34		3804	7809	bdl
T4–10	81.29		8835	23000	114
T4–15	61.38		16000	45000	219
T4–17	72.73		16000	46000	194
T4–20	40.61		18000	54000	254
T4–30	20.77		23000	82000	295
T4–35	28.01		21000	68000	247
T4–40	21.51		22000	68000	306
T4–46	32.25		21000	68000	320
T4–50	27.84		20000	62000	295
T4–60	26.66		24000	75000	324
T4–67	29.08		21000	64000	346
T4–70	22.32		23000	71000	305
T4–80	31.04		25000	78000	345
T4–90	29.3		25000	85000	361
	Min	Max	Mean	Median	Max SD (%)
Pb (mg/kg)	2307	27,000	12,856	8835	12
Zn (mg/kg)	6583	86,000	38,605	25,000	7
Cd (mg/kg)	33	411	198	206.5	36

Basic statistics of measured soil concentrations (mg/kg) also provided

SD standard deviation, *bdl* below detection limit

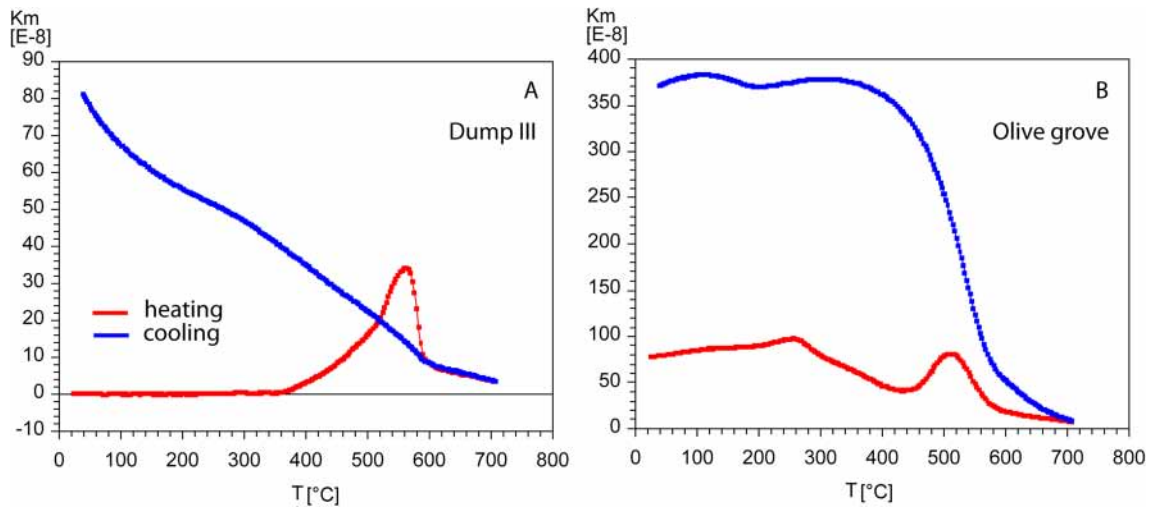


Fig. 4 Representative temperature-dependent magnetic susceptibilities curves (K–T curves) from dump III surface sample and soil from the Olive grove

parameter with the laboratory MS2B Bartington sensor (operating frequencies 0.465 kHz (LF) and 4.65 kHz (HF)), gave relatively high values for surface samples taken along profiles T1, T4, T6, and T7 in the olive grove. These values range from 7.97 to 11.3%, with a mean of $10.81 \pm 0.33\%$ for combined T6–T7 profiles and means of $9.36 \pm 0.77\%$ and $9.33 \pm 0.5\%$ for T4 and T1, respectively. Similar value range is also observed for depth profiles C1–C4 with a mean of $10.01 \pm 0.86\%$.

Maximum $\chi_{fd}\%$ values are similar in theoretical calculations and in synthetic grain data, reaching 14.5–16.9% for magnetite and 11.6–14.3% for maghemite with values of ~10–12% for a wide and equal distribution of SP grains

(Dearing et al. 1996). The tendency for higher percentage values away from the tailing (T6–T7 profiles) can be interpreted as a higher concentration of SP (titano)maghemite probably originating from the original natural uncontaminated soil while the soils closer to the tailings indicate a lower degree in SP magnetic grains in agreement with a higher content of paramagnetic and canted antiferromagnetic minerals (ferrihydrite, goethite, etc.) originating from the tailing. The same tendency to increased percentage value at depth on the profiles C1 and C4 (Fig. 5) also strengthens this interpretation. Though poorly resolved, the slight decrease at about 20 cm depth on profile C4 would in the same line of interpretation indicate a higher degree of contamination

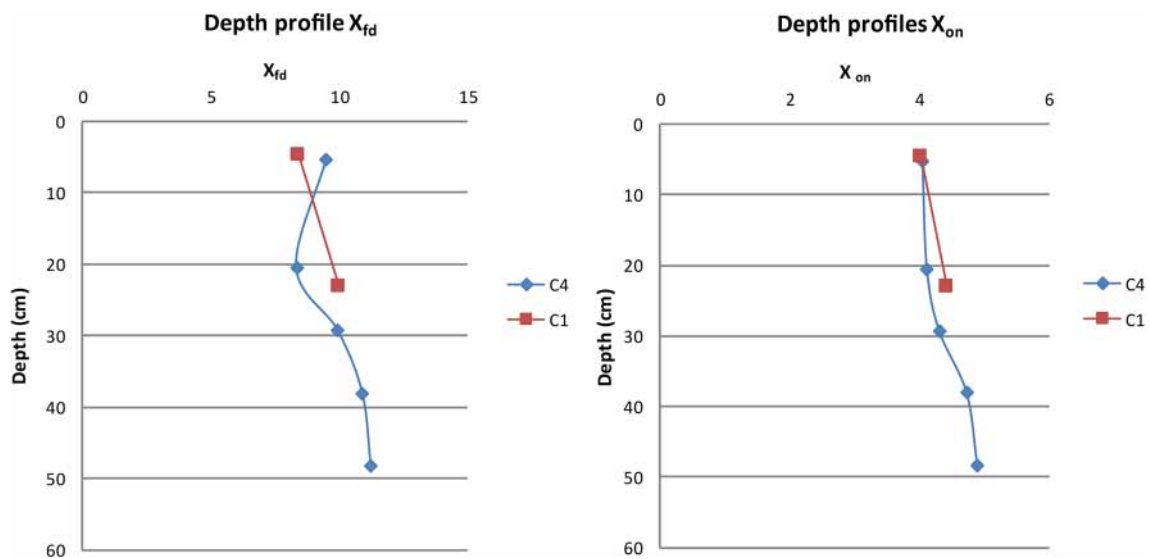


Fig. 5 Variations of the frequency-dependent parameters χ_{fd} (%) and χ_{ON} (Hrouda et al. 2013) versus depth for depth profiles C1 and C4

at depth in this part of the olive grove in accordance with the concomitance of the topographic depression previously mentioned (“Site description and sampling”).

Frequency-dependent susceptibility measurements were reproduced on a more sensible MFK1 AGICO susceptibilimeter based at the LFC (Pau, France), using the out of phase susceptibility component following the procedure described in Hrouda et al. (2013) and using the χ_{on} parameter. Comparison of the χ_{on} parameter with the $\chi_{FN(0.5, 4.5)}$ (see formula 11 in Hrouda et al. 2013) previously measured with the Bartington MS2D sensors exhibit a fairly good linear correlation ($\chi_{on} = 1.01 \chi_{FN}$, $R^2 = 0.68$) confirming the variations already observed and, therefore, the above-mentioned interpretations (Fig. 5).

4. Discussion

From the methodological point of view, the comparison on the same profiles of a given parcel of susceptibility measurements obtained with three different commercial susceptibilimeters (KT10, Bartington MS2D, GEONICS EM38) demonstrate the reliability and reproducibility of susceptibility measurements to track soil contamination and the ability of these different devices to spatialize it accurately, despite their different penetration depths. With the appropriate calibration procedure (Thiesson et al. 2016), the integration depth of about 1.5 m of the GEONICS EM38 allows to investigate the contamination at higher depths than other frequently used field susceptibilimeters. It also allows overcoming possible noise induced by small superficial contamination variations or small metallic artifacts, even if users have to be aware that the susceptibility measurements can partly integrate, like in this study, the susceptibility signal of the uncontaminated soils. We therefore demonstrate, with this dataset, the efficiency of the GEONICS EM38 for susceptibility measurements in contaminated soils studies while this specific use was up to now mainly restrained to Geoarcheology (i.e., De Smedt et al. 2014; Heil and Schmidhalter 2019). The advantage of using the GEONICS EM38 for environmental prospection, besides its investigation depth, resides in the possible combination, with a single device, of the susceptibility maps with soil resistivity ones for which the GEONICS EM 38 is mostly dedicated (i.e., Heil and Schmidhalter 2019). The commercial Terraplus KT10 and MS2D Bartington susceptibilimeters (even if known for their slightly lower sensitivity compared to laboratory susceptibilimeters) also proved their reliability even in the case of very low intensity signal rarely reported to our knowledge in the literature. This is evidenced by the good correlation between the laboratory and field data which allowed us to realize a combined map following the failure of the Bartington MS2D sensor in the field for profiles T6 and T7 .

Besides the metrological contribution, this study also displays a very rare case of proven anti-correlation between magnetic susceptibility measurements and soil contamination successful in detecting metallic pollution. Magnetic studies in soils from various contaminated environments worldwide often report enhancement of the magnetic susceptibility (and/or other related magnetic parameters) positively correlated with increased metals content (for Zn, Pb, Ni, and Cu, see, for example, Dankoub et al. 2012; Bourliva et al. 2016; Attoucheik et al. 2017; Magiera et al. 2018; Wang et al. 2018; Chaparro et al. 2020 for recent publications). However, spatialization of a metallic contamination in soils with the reverse behavior is reported here for the first time to our knowledge in the literature. This anti-correlation case is nevertheless very robust as a tracer of this contamination and corroborated by our pXRF data. Our mineralogical results obtained on dumpD III (both from thin section and magnetic properties) clearly indicate the feeble concentration of ferromagnetic carriers in the mining waste characterized by a ‘low’ magnetic signal. The iron oxyhydroxides are mainly amorphous such as ferrihydrite with a minor component of most probably maghemite coming from slow transformation at low temperature and low pH. In the olive grove, the relatively higher magnetic susceptibilities (compared to those of the mining waste) found in the surface samples (profiles T1–T4 and T6–T7) and their associated magnetic properties show a higher contribution of (titano)maghemite of natural origin probably originating from mixing with the initial uncontaminated soils, potentially increased by the plowing. Nevertheless, in most of the olive grove and especially on the susceptibility maps of the ‘shallow susceptibilimeters’, the intensity of signal, below the range of magnetic susceptibilities measured in uncontaminated matrix ($100\text{--}150 \times 10^{-5}$ SI), allow to visualize the extent of contamination to at least more than 200 m from dump DIII (see Fig. 2) in accordance with the previous findings from mineralogical and geochemical investigations (Souissi et al. 2015; Béjaoui et al. 2016). At depth, the magnetic properties on profile C4 evidence a strong decrease of the detectable contamination below about 50 cm corroborated by pXRF data. Souissi et al. (2015) also show a strong decrease in Pb, Zn and Cd between 50 and 70 cm on a depth profile realized about 200 m from the flotation tailings dump DIII (PR7 on Fig. 1). The localization of the profile PR7 (Souissi et al. 2015) and C4 (this publication) are about 50 m apart and lie on the same susceptibility contour on the magnetic susceptibility map produced with the GEONICS EM38. This further confirms the magnetic susceptibility and heavy metal contamination reverse correlation as an accurate qualitative tool, both at surface and depth, for Pb, Zn, and Cd concentrations. A reassessment of these findings following the methods from the ISO21226:2019 would be the next step to refine the use of magnetic susceptibility to trace soil

contamination and extend its use even in cases of very low signal (International Organization for Standardization 2019. Soil Quality—Guideline for the Screening of Soil Polluted with toxic elements using Soil Magnetometry (ISO Standard No. 21226:2019)).

Concerning the mechanism for contaminant dispersion, the interpretation of the susceptibility maps from the olive grove evidences the impact of rainfall transfer and topography (see “[Magnetic properties and anti-correlation with contamination](#)”) in the dispersion and accumulation of the contaminants in this area west of the dump. Aeolian processes also play a role (Ghorbel et al. 2014), like in other contexts (see Pierwola et al. 2020 for example), but localization of the highest contamination levels along two observed pathways corresponding to streaming water line (or temporary brooks) linking a central depression zone to the dump slope favor rainfall transfer as the dominant mechanism for the contamination repartition. Magnetic susceptibility map realized with the EM38 susceptibilimeter evidences a high degree of contamination reaching up to 150 cm depth (integration depth of the device) in localized areas exhibiting minimum values around $10 \cdot 10^{-5}$ SI (Fig. 2) as found on the top of Dump III (profile D3). Values, one order of magnitude higher and similar to those of the measured unpolluted soil matrix, localize mostly on the North Western Edge of the map and indicate a progressing vanishing of the impregnation at depth of the contamination. This further confirms the ‘almost’ 3D mapping potential of the magnetic susceptibility field data.

Health risk assessment in these agricultural soils near former mining sites remains the ultimate goal for mapping contamination with geophysical methods. For olive grove surrounding Jebel Ressay, Béjaoui et al. (2016) found that all olive samples had Pb concentrations above limits (i.e., 0.1 mg/kg WW—Commission Regulation (EC) No 1881/2006 of 19 December 2006 setting maximum levels for certain contaminants in foodstuffs (Text with EEA relevance). Indeed, for the olive grove concerned by this study, olive sample JR4 shows Pb contents of 0.168 mg/kg WW, while content in Cd is 0.018 mg/kg WW (below recommended limit of 0.05 mg/kg WW). They also point out the extreme values of sample JR3 situated just west of profile T5–T6 of the investigated zone (Fig. 1), where susceptibility maps exhibit a maximum degree of contamination both in the sub-surface and at depth. However, these authors also point out that if a good correlation between olive Cd content and total surface soil content is found, olive Pb content is not correlated to total surface soil content (Béjaoui et al. 2016). If transfer in fruit not simply related to Pb content concentration in soils can be invoked as done by Béjaoui et al. (2016), another hypothesis may arise from the geophysical measurements. On the susceptibility maps, the position of the JR4 samples lies on the $55\text{--}60 \cdot 10^{-5}$ SI, $35 \cdot 10^{-5}$ SI and

$30 \cdot 10^{-5}$ SI contours for the Terraplus KT10, Bartington MS2D, and Geonics EM38 sensors, respectively. Given the increasing integration depths of the devices and the low susceptibilities recorded with the Geonics EM38, this may indicate an increasing impregnation at depth of the contaminants with a lower concentration on the surface layer [which were sampled in the Béjaoui et al. (2016) study] compared to more deeper ones. Olive trees are known to have a shallow root system developed principally in the first meter (mainly between 60 and 100 cm). In a different context, Petrovsky et al. (2001) also reported a better correlation between magnetic susceptibility and heavy metal content (Pb, Cd and Zn) at depth versus surface in alluvial soils formed after breakdown of a dam lagoon with deposited ashes of a lead ore smelter. The absence of correlation between Pb total surface soil content and olive Pb content could, therefore, be linked to Pb soil content at depth, which might differ from the surface one and then further strengthen the need for a more 3D vision of the contamination. Geophysical methods as exemplified here combined with selected geochemical analysis could in this way provide important constraints for bioaccessibility studies and in turn to health risk assessments and tuning of agricultural practices.

In turn, the good correlation (0.85) between Olive Cd content and total surface soil content could indicate a more homogenous distribution in the soil linked to different transfer mechanisms of this element between surface and depth in this context or a lower efficiency of the magnetic methods in tracing this contaminant. If numerous studies document good correlations between Cd content in soil and magnetic susceptibility worldwide (see, for example, Petrovsky et al. 2001; Pérez et al. 2014; Magiera et al. 2018; Rai et al. 2019 among other) more rarely poor correlation can also be reported (Karimi et al 2011). It is noticeable that in this study, lower determination coefficients R^2 are found for correlation of magnetic susceptibilities with Cd content compared to Zn and Pb. Further investigating processes like surface complexation to iron oxyhydroxides (Palumbo-Roe et al. 2009; McCann et al. 2015) is needed to better resolve this issue and refine interpretations of the susceptibility maps but is beyond the scope of this paper.

Conclusions

The realization of magnetic susceptibility maps with three different commercial susceptibilimeters (Terraplus KT10, Bartington MS2D, Geonics EM38) in olive grove soils contaminated with heavy metals (mainly Pb, Zn, and Cd) dispersed from adjacent tailings lead to the following conclusions :

- Evidence of a rare case of proved reverse correlation of magnetic susceptibility and heavy metal contamination.
- Demonstration of the ability and coherency of the different susceptibilimeters as quick and cost-effective tools for spatializing the contamination even at very low signal and, therefore, constituting a decision predictive tool to reduce the number of more costly analyses.
- The contamination distribution as imaged by the susceptibility maps evidence the impact of rainfall transfer and topography as the specific transfer mechanisms in these carbonated soils under semi-arid climate leading to contaminant soil enrichment in the investigated area.
- With a proper calibration, and due to its investigation depth, the Geonics EM38 revealed an efficient tool for spatializing the contamination at depth and coupled with shallower susceptibilimeters provides a qualitative 3D imaging of the contamination to be used notably for elements mobility and bioaccessibility studies.

This study demonstrates that even in this particular industrial and environmental combination, susceptibility even with a very low signal remains a performant, quick, and cost-effective tool for spatializing soil contamination and combined with selected geochemical analysis can provide important constraints on heavy metals mobility and bioaccessibility, to be taken into account for adaptation of agricultural practices.

Acknowledgements The authors thank the editor and reviewers for their careful reading and comments that greatly improved the manuscript. They also like to acknowledge N. Herrero and C. Djebbi for helping in the field and N. Herrero for Magnetic analyses. We also thank Julien Thiesson (METIS, UMR7619, Paris, France) for helping with the calibration of the GEONICS-EM38

Author contributions MM and SR performed the funding acquisition. All authors realized the investigation in the field. SR and ML designed investigation, methodology and realized interpretation. MG, MM, MS, EJ contributed to the validation of interpretation. SR and ML realized the original draft later reviewed by all other authors.

Funding This study was supported by the project PHC UTIQUÉ N° 09G 1003 and the Institut de Recherche pour le développement (IRD).

Data availability The datasets created for this current study and not provided in the text are available from the corresponding author on reasonable request.

Declarations

Conflict of interest The authors have no relevant financial or non-financial interests to disclose.

Open Access This article is licensed under a Creative Commons Attribution 4.0 International License, which permits use, sharing, adaptation, distribution and reproduction in any medium or format, as long as you give appropriate credit to the original author(s) and the source, provide a link to the Creative Commons licence, and indicate if changes were made. The images or other third party material in this article are included in the article's Creative Commons licence, unless indicated

otherwise in a credit line to the material. If material is not included in the article's Creative Commons licence and your intended use is not permitted by statutory regulation or exceeds the permitted use, you will need to obtain permission directly from the copyright holder. To view a copy of this licence, visit <http://creativecommons.org/licenses/by/4.0/>.

References

- Adriano DC (2001) Trace elements in terrestrial environments: biogeochemistry. Bioavailability and risks of metals, 2nd edn. Springer, New York. <https://doi.org/10.1007/978-0-387-21510-5>
- Atoucheik L, Jordanova N, Bayou B, Lagroix F, Jordanova D, Maouche S, Henry B, Boutaleb A (2017) Soil metal pollution from former Zn–Pb mining assessed by geochemical and magnetic investigations: case study of the Bou Caid area (Tissamsilt, Algeria). *Environ Earth Sci*. <https://doi.org/10.1007/s12665-017-6622-9>
- Béjaoui I, Kolsi-Benzima N, Sappin-Didier V, Munoz M (2016) Health risk assessment in calcareous agricultural soils contaminated by metallic activity under Mediterranean climate. *Clean: Soil, Air, Water* 44(10):1385–1395. <https://doi.org/10.1002/clen.201500512>
- Berntsen P, Park CY, Rothen-Rutishauser B, Tsuda A, Sager TM, Molina RM, Donaghey TC, Alencar AM, Kasahara DI, Ericsson T, Millet EJ, Swenson J, Tschumperlin DJ, Butler JP, Brain JD, Fredberg JJ, Gehr P, Zhou EH (2010) Biomechanical effects of environmental and engineered particles on human airway smooth muscle cells. *J R Soc Interface* 7:S331–S340. <https://doi.org/10.1098/rsif.2010.0068.focus>
- Bourliva A, Papadopoulou L, Aidona E (2016) Study of road dust magnetic phases as the main carrier of potentially harmful trace elements. *Sci Total Environ* 553:380–391. <https://doi.org/10.1016/j.scitotenv.2016.02.149>
- Boussen S, Soubrand M, Bril H, Ouerfelli K, Abdeljaouad S (2013) Transfer of lead, Zinc, and cadmium from mine tailings to wheat (*Triticum aestivum*) in carbonate Mediterranean (Northern Tunisia) soils. *Geoderma* 192:227–236. <https://doi.org/10.1016/j.geoderma.2012.08.029>
- Chaparro MAE, Nunez H, Lirio JM, Gogorza CSG, Sinito AM (2007) Magnetic screening and heavy metal pollution studies in soils from Marambio Station, Antarctica. *Antarctic Sci* 19(3):379–393. <https://doi.org/10.1017/S0954102007000454>
- Chaparro MAE, Ramirez-Ramirez M, Chaparro MAE, Miranda-Avilés R, Puy-Alquiza MJ, Böhnelt HN, Zanor GA (2020) Magnetic parameters as proxies for anthropogenic pollution in water reservoir sediments from Mexico: an interdisciplinary approach. *Sci Total Environ* 700:134343. <https://doi.org/10.1016/j.scitotenv.2019.134343>
- Daldoul G, Souissi R, Souissi F, Jemmali N, Chakroun HK (2015) Assessment and mobility of heavy metals in carbonated soils contaminated by old mine tailings in north Tunisia. *J Afr Earth Sci* 110:150–159. <https://doi.org/10.1016/j.afrearsce.2015.06.004>
- Dankoub Z, Ayoubi S, Khademi H, Lu SG (2012) Spatial distribution of magnetic properties and selected heavy metals in calcareous soils as affected by land use of Isfahan region, Central Iran. *Pedosphere* 22(1):33–47. [https://doi.org/10.1016/S1002-0160\(11\)60189-6](https://doi.org/10.1016/S1002-0160(11)60189-6)
- De Smedt P, Saey T, Meerschman E, De Reu J, De Clercq W, Van Meirvenne M (2014) Comparing apparent magnetic susceptibility measurements of a multi-receiver EMI sensor with topsoil and profile magnetic susceptibility data over weak magnetic anomalies. *Archaeol Prospect* 21:103–112. <https://doi.org/10.1002/arp.1467>

- Dearing JA, Dann RJL, Hay K, Lees JA, Loveland PJ, Maher BA, O'Grady K (1996) Frequency-dependent susceptibility measurements of environmental materials. *Geophys J Int* 124:228–240. <https://doi.org/10.1111/j.1365-246X.1996.tb06366.x>
- Ding C, Ma Y, Li X, Zhang T, Wang X (2018) Determination and validation of soils thresholds for cadmium based on food quality standard and risk assessment. *Sci Total Environ* 619–620:700–706. <https://doi.org/10.1016/j.scitotenv.2017.11.137>
- Doumas P, Munoz M, Banni M, Becerra S, Bruneel O, Casiot C, Cleyet-Marel JC, Gardon J, Noack Y, Sappin-Didier V (2018) Polymetallic pollution from abandoned mines in Mediterranean regions: a multidisciplinary approach to environmental risks. *Reg Environ Changes* 18(3):677–692. <https://doi.org/10.1007/s10113-016-0939-x>
- Dunlop DJ, Özdemir Ö (2001) *Rock magnetism: fundamentals and frontiers*, vol 3. Cambridge University Press, Cambridge
- EC No 1881/2006 Setting maximum levels for certain contaminants in foodstuffs. *Off. J. Eur. Union* 2006,19/12/2006, R1881, 5–24. <https://eur-lex.europa.eu/LexUriServ/LexUriServ.do?uri=OJ:L:2006:364:0005:0024:FR:PDF>
- Elouear Z, Bouhamed F, Boujelben N, Bouzid J (2016) Assessment of toxic metals dispersed from improperly disposed tailing, Jebel Ressas mine, NE Tunisia. *Environ Earth Sci* 75:254. <https://doi.org/10.1007/s12665-015-5035-x>
- Evans M, Heller F (2003) *Environmental magnetism*. Academic Press, Elsevier Science, New York, p 293
- Fosmire GJ (1990) Zinc toxicity. *Am J Clin Nutr* 51:225–227. <https://doi.org/10.1093/ajcn/51.2.225>
- Gendler TS, Shcherbakov VP, Dekkers MJ, Gapeev AK, Gribov SK, McClelland E (2005) The lepidocrocite–maghemite–haematite reaction chain—I. Acquisition of chemical remanent magnetization by maghemite, its magnetic properties and thermal stability. *Geophys J Int* 160:815–832. <https://doi.org/10.1111/j.1365-246X.2005.02550.x>
- Ghorbel M (2012) Contamination métallique issue des déchets de l'ancien site minier de Jebel Ressas: modélisation des mécanismes de transfert et conception de cartes d'aléa post-mine dans un contexte carbonaté et sous un climat semi-aride. Evaluation du risque pour la santé humaine. Ph.D. thesis. Tunis El Manar Univ (Tunisia) and Toulouse III Univ (France)
- Ghorbel M, Munoz M, Courjault-Radé P, Destrigneville C, de Parseval P, Souissi R, BenMammou A, Abdeljaouad S (2010) Health risk assessment for human exposure by direct ingestion of Pb, Cd, Zn bearing dust in the former miner's village of Jebel Ressas (NE Tunisia). *Eur J Min* 22:639–649. <https://doi.org/10.1127/0935-1221/2010/0022-2037>
- Ghorbel M, Munoz M, Solmon F (2014) Health hazard prospecting by modeling wind transfer of metal bearing dust from mining waste dumps: application to Jebel Ressas Pb–Zn–Cd abandoned mining site (Tunisia). *Environ Geochem Health* 36:935–951. <https://doi.org/10.1007/s10653-014-9610-y>
- Gutiérrez M, Mickus K, Mar Camacho L (2016) Abandoned Pb–Zn mining wastes and their mobility as proxy to toxicity: a review. *Sci Total Environ* 565:392–400. <https://doi.org/10.1016/j.scitotenv.2016.04.143>
- Hansard R, Maher BA, Kinnersley R (2011) Biomagnetic monitoring of industry-derived particulate pollution. *Environ Pollut* 159:1673–1681. <https://doi.org/10.1016/j.envpol.2011.02.039>
- Heil K, Schmidhalter U (2019) Theory and guidelines for the application of the geophysical sensor EM38. *Sensors* 19:4293. <https://doi.org/10.3390/s19194293>
- Horta A, Malone B, Stockmann U, Minasny B, Bishop TFA, McBratney AB, Palleser R, Pozza L (2015) Potential of integrated field spectroscopy and spatial analysis for enhanced assessment of soil contamination: a prospective review. *Geoderma* 241–242:180–209. <https://doi.org/10.1016/j.geoderma.2014.11.024>
- Hrouda F, Pokorný J, Ježek J, Chadima M (2013) Out-of-phase magnetic susceptibility of rocks and soils: a rapid tool for magnetic granulometry. *Geophys J Int* 194:170–181. <https://doi.org/10.1093/gji/ggt097>
- Hrouda F, Pokorný J, Chadima M (2015) Limits of out-of-phase magnetic susceptibility in magnetic granulometry of rocks and soils. *Stud Geophys Geod* 59:294–308. <https://doi.org/10.1007/s1200-014-0948-5>
- International Organization for Standardization (2019) *Soil quality—guideline for the screening of soil polluted with toxic elements using soil magnetometry (ISO Standard No. 21226:2019)*
- Jackson M (2003) Imaginary susceptibility, a primer. *IRM Q* 13(1):10–11
- Jemmali N, Souissi F, Vennemann TW, Carrenza EJM (2011) Genesis of the Jurassic carbonated-hosted Pb–Zn deposits of Jebel Ressas (North Eastern Tunisia): evidence from mineralogy, petrography and trace metal contents and isotope (O, C, S, Pb) geochemistry. *Resource. Geology* 61(4):367–383. <https://doi.org/10.1111/j.1751-3928.2011.00173.x>
- Johnson RH, Blowes DW, Robertson WD, Jambor JL (2000) The hydrogeochemistry of the nickel rim mine tailings impoundment, Sudbury, Ontario. *J Contam Hydrol* 41:49–80. [https://doi.org/10.1016/S0169-7722\(99\)00068-6](https://doi.org/10.1016/S0169-7722(99)00068-6)
- Jordanova D, Veneva L, Hoffmann V (2003) Magnetic susceptibility screening of anthropogenic impact on the Danube river sediments in northwestern Bulgaria—preliminary results. *Stud. Geophys Geod* 47:403–418. <https://doi.org/10.1111/j.1365-246X.2009.4315.x>
- Jordanova D, Jordanova N, Petrov P, Tsacheva T (2010) Soil development of three Chernozem-like profiles from North Bulgaria revealed by magnetic studies. *CATENA* 83(2–3):158–169. <https://doi.org/10.1016/j.catena.2010.08.008>
- Jordanova D, Jordanova N, Werban U (2013) Environmental significance of magnetic properties of Gley soils near Rosslau (Germany). *Environ Earth Sci* 69:1719–1732. <https://doi.org/10.1007/s12665-012-2006-3>
- Kabata-Pendias A (2004) Soil-plant transfer of trace elements—an environmental issue. *Geoderma* 122:143–149. <https://doi.org/10.1016/j.geoderma.2004.01.004>
- Kabata-Pendias A, Pendias H (1992) *Trace elements in soils and plants*, 2nd edn. CRC Press, Boca Raton
- Karimi R, Ayoubi S, Jalalian A, Sheik-Hosseini AR, Ayuni M (2011) Relationship between magnetic susceptibility and heavy metals in urban topsoils in the arid region of Isfahan, Central Iran. *J Appl Geophys* 74:1–7. <https://doi.org/10.1016/j.appgeo.2011.02.009>
- Lecoanet H, Leveque F, Segura S (1999) Magnetic susceptibility in environmental applications: comparison of field probes. *Phys Earth Planet Inter* 115:191–204. [https://doi.org/10.1016/S0031-9201\(99\)00066-7](https://doi.org/10.1016/S0031-9201(99)00066-7)
- Liu H, Li P, Zhu M, Wei Y, Sun Y (2007) Fe(II)-induced transformation from ferrihydrite to lepidocrocite and goethite. *J Solid State Chem* 180:2121–2128. <https://doi.org/10.1016/j.jssc.2007.03.022>
- Magiera T, Zawadzki J, Szuszkiewicz M, Fabijanczyk P, Steinnes E, Fabian K, Miszczak E (2018) Impact of an iron mine and a nickel smelter at the Norwegian/Russian border close to the Barents Sea on surface soil magnetic susceptibility and content of potentially toxic elements. *Chemosphere* 195:48–62. <https://doi.org/10.1016/j.chemosphere.2017.12.060>
- Maher BA (2009) Rain and dust: magnetic records of climate and pollution. *Elements* 5(4):229–234. <https://doi.org/10.2113/gselements.5.4.229>

- Maier G, Scholger R, Schön J (2006) The influence of soil moisture on magnetic susceptibility measurements. *J Appl Geophys* 59(2):162–175. <https://doi.org/10.1016/j.jappgeo.2005.10.001>
- McCann CM, Gray ND, Tourney J, Davenport RJ, Wade M, Finlay N, Hudson-Edwards KA, Johnson KL (2015) Remediation of a historically Pb Contaminated soil using a model natural Mn oxide waste. *Chemosphere* 138:211–217. <https://doi.org/10.1016/j.chemosphere.2015.05.054>
- Monneron-Gyurits M, Soubrand M, Joussein E, Courtin-Nomade A, Jubany I, Casas S, Bahi N, Faz A, Gabarron M, Acosta JA, Martinez-Martinez S (2020) Investigating the relationship between speciation and oral/lung bioaccessibility of a highly contaminated tailing: contribution in health risk assessment. *Environ Sci Pollut Res* 27(32):40732–40748. <https://doi.org/10.1007/s11356-020-10074-x>
- Othmani MA, Souissi F, Benzaazoua M, Bouzazhah H, Bussiere B, Mansouri A (2013) The geochemical behaviour of mine tailings from the Touiref Pb–Zn District in Tunisia in weathering cells leaching tests. *Mine Water Environ* 32:28–41
- Özdemir Ö (1990) High-temperature hysteresis and thermoremanence of single-domain maghemite. *Phys Earth Planet Inter* 65:125–136. [https://doi.org/10.1016/0031-9201\(90\)90081-8](https://doi.org/10.1016/0031-9201(90)90081-8)
- Palumbo-Roe B, Klinck B, Banks V, Quigley S (2009) Prediction of the long-term performance of abandoned lead zinc mine tailings in a Welsh catchment. *J Geochem Explor* 100:169–181. <https://doi.org/10.1016/j.gexplo.2008.05.003>
- Pankhurst QA, Pollard RJ (1992) Structural and magnetic properties of ferrihydrite. *Clays Clay Miner* 40(3):268–272. <https://doi.org/10.1346/CCMN.1992.0400303>
- Pascaud G, Boussem S, Soubrand M, Joussein E, Fondaneche P, Abdeljaouad S, Bril H (2015) Particulate transport and risk assessment of Cd, Pb and Zn in a Wadi contaminated by runoff from mining wastes in a carbonated semi-arid context. *J Geochem Explor* 152:27–36. <https://doi.org/10.1016/j.gexplo.2015.01.009>
- Passariello B, Giuliano V, Quaresima S, Barbaro M, Caroli S, Forte G, Carelli G, Iavicoli I (2002) Evaluation of the environmental contamination at an abandoned mining site. *Microchem J* 73:245–250. [https://doi.org/10.1016/S0026-265X\(02\)00069-3](https://doi.org/10.1016/S0026-265X(02)00069-3)
- Pérez I, Romero FM, Zampora O, Gutierrez-Ruiz ME (2014) Magnetic susceptibility and electrical conductivity as a proxy for evaluating soil contaminated with arsenic, cadmium and lead in a metallurgical area in the San Luis Potosi State, Mexico. *Environ Earth Sci* 72:1521–1531. <https://doi.org/10.1007/s12665-014-3057-4>
- Petrovsky E, Kapicka A (2006) On determination of the Curie point from thermomagnetic curves. *J Geophys Res* 111:B12S27. <https://doi.org/10.1029/2006JB004507>
- Petrovsky E, Kapicka A, Jordanova N, Boruvka L (2001) Magnetic properties of alluvial soils contaminated with lead, zinc and cadmium. *J Appl Geophys* 48:127–136. [https://doi.org/10.1016/S0926-9851\(01\)00085-4](https://doi.org/10.1016/S0926-9851(01)00085-4)
- Pierwola J, Szuszkiewicz M, Cabala J, Jochymczyk K, Zogal B, Magiera T (2020) Integrated geophysical and geochemical methods applied for recognition of acid waste drainage (AWD) from Zn–Pb post-flotation tailing pile (Olkusz, southern Poland). *Environ Sci Pollut Res* 27:16731–21674. <https://doi.org/10.1007/s11356-020-08195-4>
- Rai AK, Singh AK, Pati JK, Gupta S, Chakarvorty M, Nivogi A, Pandey A, Dwivedi MM, Pandey K, Prakash K (2019) Assessment of topsoil contamination in an urbanized interfluvial region of Indo-Gangetic Plains (IGP) using magnetic measurements and spectroscopic techniques. *Environ Monit Assess* 191:403. <https://doi.org/10.1007/s10661-019-7525-x>
- Sainfeld P (1952) Les gîtes plombo-zincifère de la Tunisie. *Ann Des Mines Et De La Géol* 9:72–78
- Schmidt A, Yarnold R, Hill M, Ashmore M (2005) Magnetic susceptibility as proxy for heavy metal pollution: a site study. *J Geochem Explor* 85:109–117. <https://doi.org/10.1016/j.gexplo.2004.12.001>
- Sliti N, Abdelkrim C, Ayed L (2019) Assessment of tailings stability and soil contamination of Kef Ettout (NW Tunisia) abandoned mine. *Arab J Geosci* 12:73. <https://doi.org/10.1007/s12517-018-4204-0>
- Soubrand-Colin M, Horen H, Courtin-nomade A (2009) Mineralogical and magnetic characterisation of iron titanium oxides in soils developed on two various basaltic rocks under temperate climate. *Geoderma* 149:27–32
- Souissi R, Souissi F, Ghorbel M, Munoz M, Courjault-Radé P (2015) Mobility of Pb, Zn, and Cd, in a soil developed on a carbonated bedrock in a semi-arid climate and contaminated by Pb-Zn tailing, Jebel Ressay (NE Tunisia). *Environ Earth Sci* 73:3501–3512. <https://doi.org/10.1007/s12665-014-3634-6>
- Steeple DW (2001) Engineering and environmental geophysics at the millennium. *Geophysics* 66:31–35
- Tauxe L (1998) Paleomagnetic principles and practice. Modern approaches in geophysics. Kluwer Academic Publishers, Amsterdam
- Tauxe L (2005) Essentials of paleomagnetism. University of California Press, Tomlinson
- Thiesson J, Kessouri P, Schamper C, Tabbagh A (2016) Calibration of frequency-domain electromagnetic devices used in near surface surveying. *Near Surf Geophys* 12:481–491. <https://doi.org/10.3997/1873-0604.2014012>
- USEPA (2012) National primary drinking water regulations
- Verosub KL, Roberts AP (1995) Environmental magnetism past, present and future. *J Geophys Res Solid Earth* 100:2175–2192
- Wang XS (2013) Assessment of Heavy metal pollution in Xuzhou urban topsoils by magnetic susceptibility measurements. *J Appl Geophys* 92:76–83. <https://doi.org/10.1016/j.jappgeo.2013.02.015>
- Wang B, Xia D, Yu Y, Chen H, Jia J (2018) Source apportionment of soil-contamination in Baotou City (North China) based on a combined magnetic and geochemical approach. *Sci Total Environ* 642:95–104. <https://doi.org/10.1016/j.scitotenv.2018.06.050>

Publisher's Note Springer Nature remains neutral with regard to jurisdictional claims in published maps and institutional affiliations.